Hydrometeor charges observed below an electrified cloud using a new instrument

Qixu Mo,[1] Andrew G. Detwiler,[2] John Helsdon,[2] W. P. Winn,[3] G. Aulich,[4] and W. Clifton Murray[5]

Received 20 July 2006; revised 19 January 2007; accepted 28 January 2007; published 11 July 2007.

[1] Investigation of charges on particles in thunderstorms was conducted during the Severe Thunderstorm Electrification and Precipitation Study. In the case presented here, aircraft measurements of the electric field, and hydrometeor size and charge, were made in a precipitation shaft beneath the base of a small convective cloud which was electrified, but which produced no lightning. A newly designed instrument was used to obtain particle image and charge measurements for particles larger than 0.2 mm in size. Laboratory tests and calculations suggest that under optimum conditions particle charge can be determined with this instrument to within 13% for particles carrying more than a few pC of charge. Uncertainty in charge magnitude increases to 24% in less optimum conditions. It was found in this shower of melting graupel with a peak concentration of ~80 particles m^{-3} that 70% of the particles were charged, with 98% of the charged particles having positive charge. Peak particle sizes were 2 mm, and peak charges were 25 pC. The magnitude of charge varied widely for particles of a given size, but minimum, average, and maximum charge generally increased as particle size increased. The hydrometeors in this region constituted a lower positive charge center. This center must have developed through microphysical interactions and not charge transferred by lightning discharges.

Citation: Mo, Q., A. G. Detwiler, J. H. Helsdon, W. P. Winn, G. Aulich, and W. C. Murray (2007), Hydrometeor charges observed below an electrified cloud using a new instrument, *J. Geophys. Res.*, *112*, D13207, doi:10.1029/2006JD007809.

1. Introduction

[2] Knowledge of the types of particles carrying charge in electrified clouds, and of the relationship between charge and size, can help to decide whether proposed thunderstorm electrification mechanisms actually contribute to electrification of thunderstorms. For example, the currently favored hypothesis is that cloud electrification begins when graupel and small ice crystals collide in the presence of cloud liquid water. This idea is based on laboratory experiments in which, under simulated cloud conditions, charge is transferred between ice crystals and a riming ice target [*Reynolds et al.*, 1957; *Takahashi*, 1978; *Jayaratne et al.*, 1983; *Saunders et al.*, 1991]. Measurements of charge on precipitation particles arriving at the ground were first made more than 100 years ago (see review by *MacGorman and Rust* [1998, chapter 6]), but such measurements reveal only a little about the important microphysical and electrical processes occurring aloft within the thunderclouds themselves. More recently, within the last 50 years, investigators have attempted to measure the charge carried by precipitation particles in situ in mixed phase and ice clouds, using aircraft and balloons.

1.1. Aircraft Observations

[3] Some of the earliest work using instrumented aircraft in the United States is described by *Gunn* [1947]. He employed an induction ring instrument to monitor hydrometeor charges in thunderstorm and nonthunderstorm clouds. *MacCready and Proudfit* [1965] discuss later airborne observations with an induction ring in northern Arizona beneath a sample of summer cumulus congestus clouds that had yet to produce lightning. *Latham and Stow* [1969] discuss more comprehensive observations of hydrometeor charge, using a similar instrument, combined with observations of ambient electric fields, within and beneath similar convective clouds in the same geographic region. *Gardiner et al.* [1985], *Dye et al.* [1986], *Brooks* [1993] and *Bringi et al.* [1997] report airborne observations within thunderstorms in Montana and Florida with somewhat more sophisticated induction ring instruments. This work in general showed that in many regions within and below clouds, when charged hydrometeors are present, there are charges of both signs. Occasionally there are relatively

[1] SPEC, Inc., Boulder, Colorado, USA.
[2] Institute of Atmospheric Sciences, South Dakota School of Mines and Technology, Rapid City, South Dakota, USA.
[3] Department of Physics, New Mexico Institute of Mining and Technology, Socorro, New Mexico, USA.
[4] Langmuir Laboratory, New Mexico Institute of Mining and Technology, Socorro, New Mexico, USA.
[5] Department of Mathematics and Statistics, University of New Mexico, Los Lunas, New Mexico, USA.

Copyright 2007 by the American Geophysical Union.
0148-0227/07/2006JD007809

limited regions with monopolar charge. Charge densities of up to several nC/m^3 can be observed. Significant concentrations of charged hydrometeors can exist within clouds, or in precipitation shafts below clouds, that are not producing lightning.

[4] In the work just described, separate instruments observed particle charge and particle size, if particle size was monitored at all, so an unambiguous assignment of a detected charge to a particle of a particular size and type was rarely possible. Airborne instruments combining an induction ring with optical sizing or imaging capability are described by *Gaskell et al.* [1977, 1978], *Christian et al.* [1980], *Vali et al.* [1984], *Cupal et al.* [1989], and *Weinheimer et al.* [1991]. *Gaskell et al.* [1977, 1978] discuss observations conducted within several summer thunderstorms in Florida and over the mountains of central New Mexico. *Christian et al.* [1980] describe subsequent work, with upgraded versions of the same instruments used by *Gaskell et al.* [1977, 1978], in two New Mexico summer mountain thunderstorms. Combining an induction ring device with true imaging capability leads to better capability to relate particle size and microphysical characteristics (ice versus liquid, degree of riming if ice, etc.) to particle charge. *Vali et al.* [1984], *Cupal et al.* [1989], and *Weinheimer et al.* [1991] report varying degrees of success with early airborne instruments of this type. In both cases, an induction ring was added to a two-dimensional optical imaging probe made by Particle Measuring Systems, Inc.

[5] These observations yielded results similar to those obtained earlier with induction ring devices alone concerning bipolar charge distributions, and they yielded more information on typical charge densities. In addition, they showed little correlation between particle size, type, and charge.

1.2. Balloon-Borne Observations

[6] There also is a history of making particle charge measurements using balloon-borne instruments. *Marshall and Winn* [1982] report observations within New Mexico thunderstorms from balloon-borne instrumentation capable of measuring particle charge, as well as ambient electric field. *Bateman et al.* [1994, 1995, 1999] conducted campaigns in Oklahoma and New Mexico combining in situ balloon-borne measurements of precipitation particle charge with an optical determination of size. Another instrument on the same balloon determined the ambient electric field. These observations provided more information than do aircraft observations about the vertical distribution of charge in thunderstorms. They were generally consistent with the thunderstorm charge tripole model [*Krehbiel*, 1986]. In some regions, mainly in the middle and lower portions of the convective clouds, precipitation was the dominant charge carrier, and in others, mainly higher in the cloud, much of the charge was inferred to have been on smaller ice and liquid water particles.

1.3. Need for New Observations

[7] The proposed collision mechanisms of convective cloud electrification may be separated into two categories, inductive and noninductive. For inductive mechanisms, the ambient electric field polarizes ice particle charges in such a way that particle collisions will transfer a net charge. For noninductive collision mechanisms, by contrast, with the right combination of ice particles, temperature, and cloud droplets, charge separation can occur between colliding particles without the presence of an ambient electric field. The noninductive collision mechanism is thought at present to be the dominant charge separation mechanism in thunderstorms.

[8] While detailed observations of inductive and noninductive charge separation processes have been made in controlled laboratory environments, in situ observations are obtained only in the uncontrolled and chaotic environment of an actual thunderstorm. It often is difficult to know even the most recent history/histories of the particles sampled at a particular location in a cloud. It is thus difficult to interpret microphysical and electrical properties of particles sampled in a particular region of a storm in terms of charge magnitude and sign separated during simulations of cloud processes in a controlled laboratory environment. Despite these limitations, in situ observations are necessary if we are to know what mechanism(s) is (are) responsible for cloud electrification. One important conclusion based on in situ observations made so far is that an inductive collisional charging mechanism cannot result in the observed appearance of significant charge on particles during the early stages of cloud development when the electric field everywhere in the cloud still is quite small. Another important conclusion is that neither the inductive nor noninductive collisional mechanism is consistent with the lack of relationship between charge magnitude and particle size that commonly is observed. With regard to the noninductive graupel-crystal collision hypothesis, the relationship between observations and laboratory results are ambiguous. For example, the relationship between temperature and the sign of charge acquired by the rimer in laboratory experiments, and the temperatures associated with the three charge layers of alternating sign in the standard tripolar picture of thundercloud electrical structure [*Williams*, 1989], are often in qualitative agreement. However, recent studies indicate more complex storm charge structures [*Stolzenburg et al.*, 1998; *Stolzenburg and Marshall*, 1998].

[9] In recent years, improved remote sensing technologies, including polarimetric meteorological radars and three-dimensional lightning mapping systems, allow more complete volumetric mapping of microphysical and electrical storm characteristics through entire storm life cycles. More precise and informative in situ microphysical and charge measurements are facilitated by improved instrument design, optics, electronics and processing algorithms. Global Positioning System technology allows very precise location of these in situ measurements within the storms. Thus, even though there are in the literature a number of published observations of precipitation particle charge and corresponding cloud microphysical characteristics, there is a need to present new, more quantitative and statistically robust observations. Only with such observations can laboratory results be reconciled with field observations, and numerical models of thunderstorm electrification developed and tested.

[10] Here we show a simple case in which measurements were taken along an ascending path under the base of a small collapsing cumulus congestus cloud using a novel particle imaging instrument on an airplane. In this case the

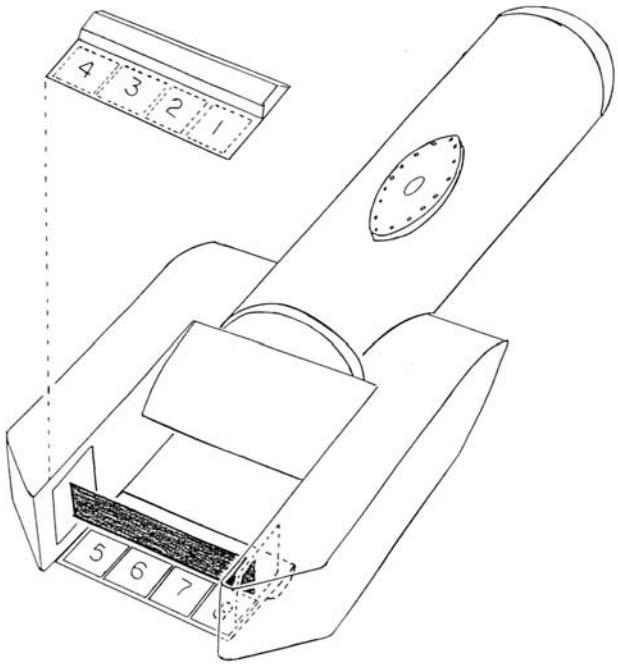

Figure 1. Sketch of High Volume Particle Sensor (HVPS) with the charge detector. The upper half of the charge detector is shown lifted out of position, in order to expose the laser beam (shaded).

charge density can be inferred both from independently calibrated aircraft-measured electric field and from individual hydrometeor charge observations, and good agreement between these instrument systems is obtained. The combination of a relatively simple cloud, and the improved size and charge sampling statistics based on instrument design and sample volume, yield insight into the charge separation processes that were ultimately responsible for the charged particles observed falling from this small cloud.

2. Instrumentation

[11] The observations presented below were obtained during the Severe Thunderstorm Electrification and Precipitation Study (STEPS) conducted in the northern part of the Colorado-Kansas border area in the summer of 2000. Among the instruments and platforms participating in this study were the Colorado State University Chicago-Illinois (CSU-CHILL), and National Center for Atmospheric Research Spol, polarimetric meteorological radars (see *Brunkow et al.* [2000] and http://www.atd.ucar.edu/dir_off/facilities/laof.html#spol, respectively), the New Mexico Institute of Mining and Technology (NMIMT) lightning mapping array (LMA) [*Rison et al.*, 1999], the Vaisala National Lightning Detection Network (NLDN), and the South Dakota School of Mines and Technology armored T-28 research aircraft [*Johnson and Smith*, 1980; http://www.ias.sdsmt.edu/institute/t28/index.htm]. The observations from the radars and lightning mapping array are used to follow the overall physical and electrical development of a small convective cloud. The airborne instruments are used to make detailed microphysical and electrical observations in limited regions under the cloud near the end of its precipitation-forming stage.

[12] The key instruments on the armored T-28 aircraft used in this study are its six electric field meters and a SPEC, Inc., HVPS (High Volume Particle Sensor) which is integrated with a particle charge detector made at the New Mexico Institute of Mining and Technology.

[13] The six electric field meters on the airplane are used to determine all three Cartesian components of the ambient field and the net charge carried by the airframe. A detailed description of the field meters, their calibration, and the computations of ambient electric field from their readings is given by *Mo et al.* [1999]. The field meter system in 2000 consisted of six meters, one more than the system described in *Mo et al.* [1999]. The additional meter added redundancy in the retrieval algorithm and facilitated overall more accurate computations of electric field components.

[14] Figure 1 shows the HVPS and its associated charge detector. The instrument is positioned below the middle point of the starboard wing of the airplane, outside the propeller wash to avoid sampling particles thrown off by the propeller. Using a laser-generated sheet of light it shadows particles on a linear photodiode array. The image sampling area is 20 cm by 5 cm. The image resolution is 0.2 mm in the vertical and 0.8 mm along the direction of flight. The charge detector consists of eight electrode plates arranged in two rows, four plates on the top row and four on the bottom row. The HVPS laser beam fills 70% of the plane between these two rows of electrodes.

[15] When a particle enters the beam area, it produces a shadow on some of the HVPS sensing diodes. This triggers the instrument to collect successive records of the diode array state in order to form an image of the particle, and also to begin recording six samples of the induced charge on each electrode plate. Image recording ends when all diodes are again illuminated. The electrode plate sampling frequency is determined by the airspeed so that the sixth sample is taken when the particle is just reaching the rear edge of the plates. A new particle cannot be recorded until charge sampling is finished. This ''dead time'' is accounted for in computation of particle and charge concentrations.

[16] As with earlier charge detectors, an induced charge signal which decays too slowly indicates either electrical noise and/or a particle moving too slowly, such as water or ice shed by the instrument itself. Such signals are rejected in the data analysis. The present charge detector's multiple-electrode design, however, enables one to do additional signal analysis and apply rejection criteria which were not possible with earlier instruments:

[17] 1. Comparison of the relative signal strengths between upper and lower electrode arrays enables one to infer the vertical location of the particle within the measurement space [*Fong and Kittel*, 1967]. This inferred location should agree with the vertical location of the image, thus reducing the chances of assigning a charge signal to the wrong image. (See below for further details.)

[18] 2. One may take the weakest of the eight electrode signals as a measure of the electrical noise, due to fluctuating ambient fields or to charging and discharging of the aircraft. This noise signal can be subtracted from the total

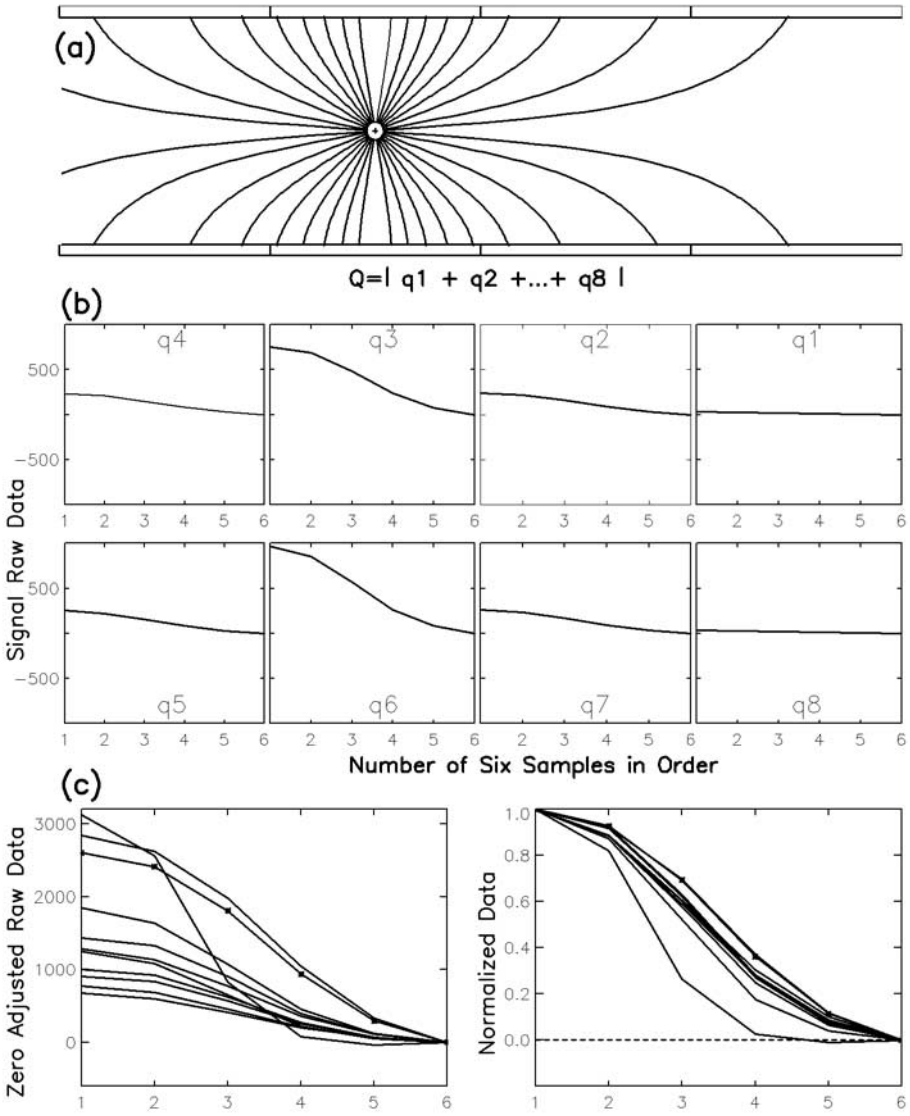

Figure 2. (a) Sketch of electric field lines for a charge between the electrodes viewed looking straight into the instrument toward the aft end of the airplane. (b) Induced charges (in arbitrary units) due to the passage of a charged metal pellet through the array of electrodes. The six samples of induced charge are connected by straight lines. The samples correspond to pellet movement of 0.8 cm relative to the electrodes. (c) Signals from 11 pellet tests. Curves in the left plot were adjusted up or down to end up at zero. Curves in the right plot were normalized to start at 1.

signal on the eight electrodes, resulting in a more accurate estimate of particle charge.

[19] 3. An acceptable measurement should be of only one particle, not two or more particles simultaneously. Examining the eight electrodes' signals can improve recognition of spurious data due to two or more particles' passing close together through the measurement space. An acceptable particle should induce its strongest signals on electrodes grouped together around its path.

[20] 4. A single particle should induce the same sign of charge on all electrodes. Two or more significant signals of opposite sign suggest multiple particles may have been in the measurement space simultaneously.

[21] The particle vertical location inferred from charge signals and the vertical location from the imaging probe are compared in the following way. According to the theoretical results of *Fong and Kittel* [1967], the relative position of a charge between two parallel capacitor plates is proportional to the ratio of the induced charges on the two plates. For example, let q_1 be the total induced charge on the top four plates of the charge detector, and q_2 be the total induced charge on both top and bottom plates, then ratio q_1/q_2 can be calculated from the charge signals. Suppose the charge is d_1 cm from the top plates and the distance between top and bottom plates is L cm, then q_1/q_2 will be equal to $(L-d_1)/L$. The particle's actual distance d_1 from the top plates can be

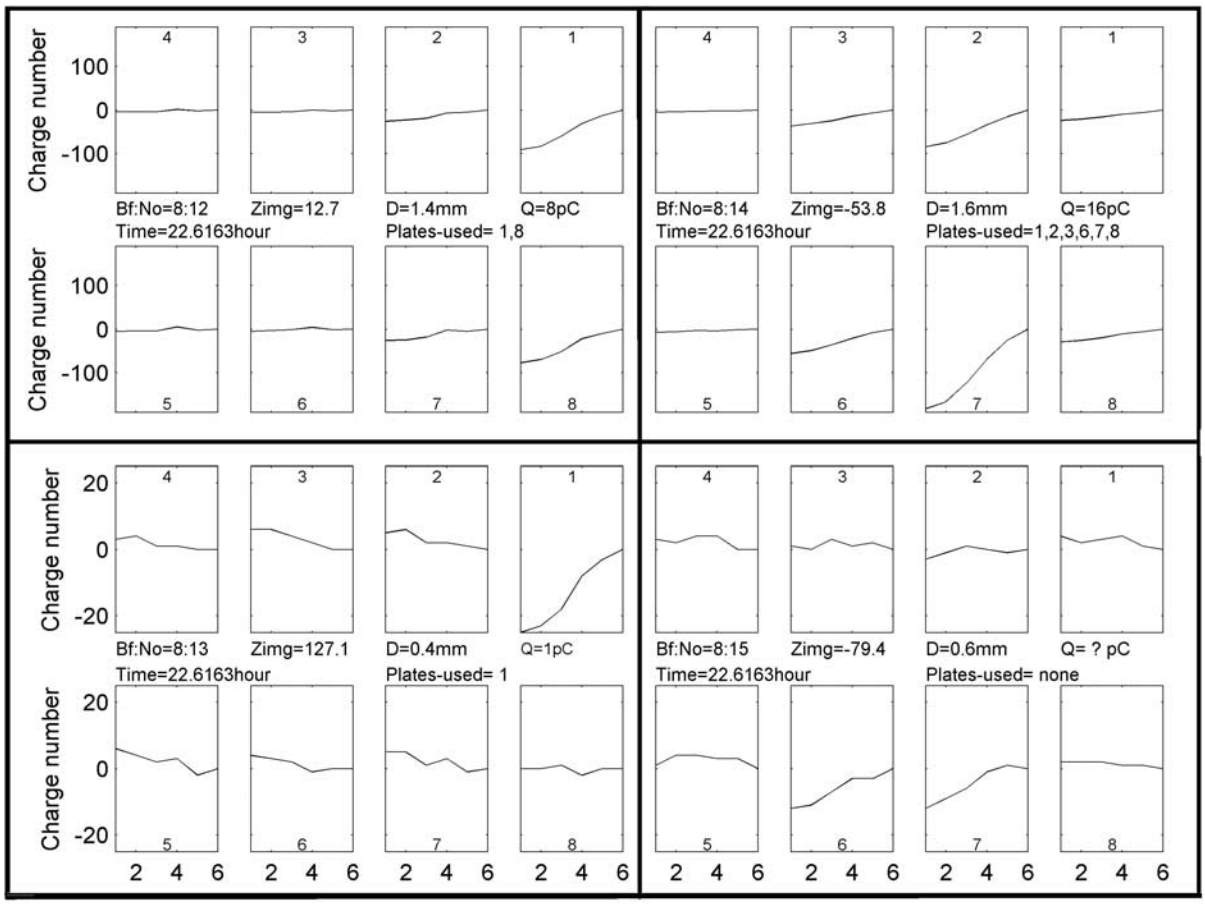

Figure 3. Four sequential particles' charge data measured in a fraction of a second in the positive charge region. Data from all eight plates for each hydrometeor passage are shown. For each plate, a signal proportional to charge induced on the plate is shown for six successive samples. The time between samples is equal to a fixed particle travel distance relative to the airplane divided by the airplane's airspeed. Charge number is the voltage-to-digital count signal recorded as the hydrometeor passed. *Bf:No* is the Buffer number and particle sequence number. One image data buffer typically contains 30 to 40 hydrometeor images from particles whose times in the data-collecting volume do not overlap. *D* is the particle's maximum vertical extent (e.g., the particle size), *Q* is the calculated charge, and *Zimg* is the vertical distance of the particle from the middle of the top row and bottom row of plates. A *Zimg* value of zero means the particle is equidistant from the top and bottom plates. A *Zimg* value of 175 means the particle is at the top edge of the laser beam. The laser beam width is 5 cm from top to bottom. The total distance between top and bottom plates is 7 cm.

determined from the image data. If the difference between q_1/q_2 and $(L\text{-}d_1)/L$ is greater than 20%, the charge data are discarded.

[22] The uncertainty in charge determination involves several factors. On the basis of tests with charged pellets, the signal from a pellet of a given charge can vary by ±12% depending on vertical position, being largest at beam center and smaller at the edges. There can be an additional uncertainty of ~5% if a charged particle passes through the beam at an angle to the horizontal, as the true charge decay profile is modulated by change in vertical position. Digitization uncertainty in recording of the charge is largest for the smallest charges. This uncertainty is ~5% for charges of 1 pC, and becomes negligible for charges of a few pC or more. Fluctuations in background signal due to nonzero charge on one or more plates when a particle enters the beam add additional uncertainty that is difficult to quantify. If we take this uncertainty to be 20% on the basis of a subjective examination of data from several clean and not-so-clean particle passages, and assume all sources of uncertainty are uncorrelated, then our estimated overall uncertainty is ~24% for particles with more than a few pC of charge in a noisy situation where background charge on the plates is hard to determine. This diminishes to ~13% for cases when the charge signals are relatively clean.

[23] Figures 2–4 illustrate how charge is determined. In Figure 2a electric field lines emanating from a charged particle terminate on the electrodes above and below the particle. Other field lines terminate on nearby parts of the airplane rather than on the electrodes, and thus the measurable sum of charges on the electrodes is less than the charge on the particle. The ratio of the charge on the particle to the total induced charge on the electrodes is a maximum when the particle is centered within the electrode array in the fore-

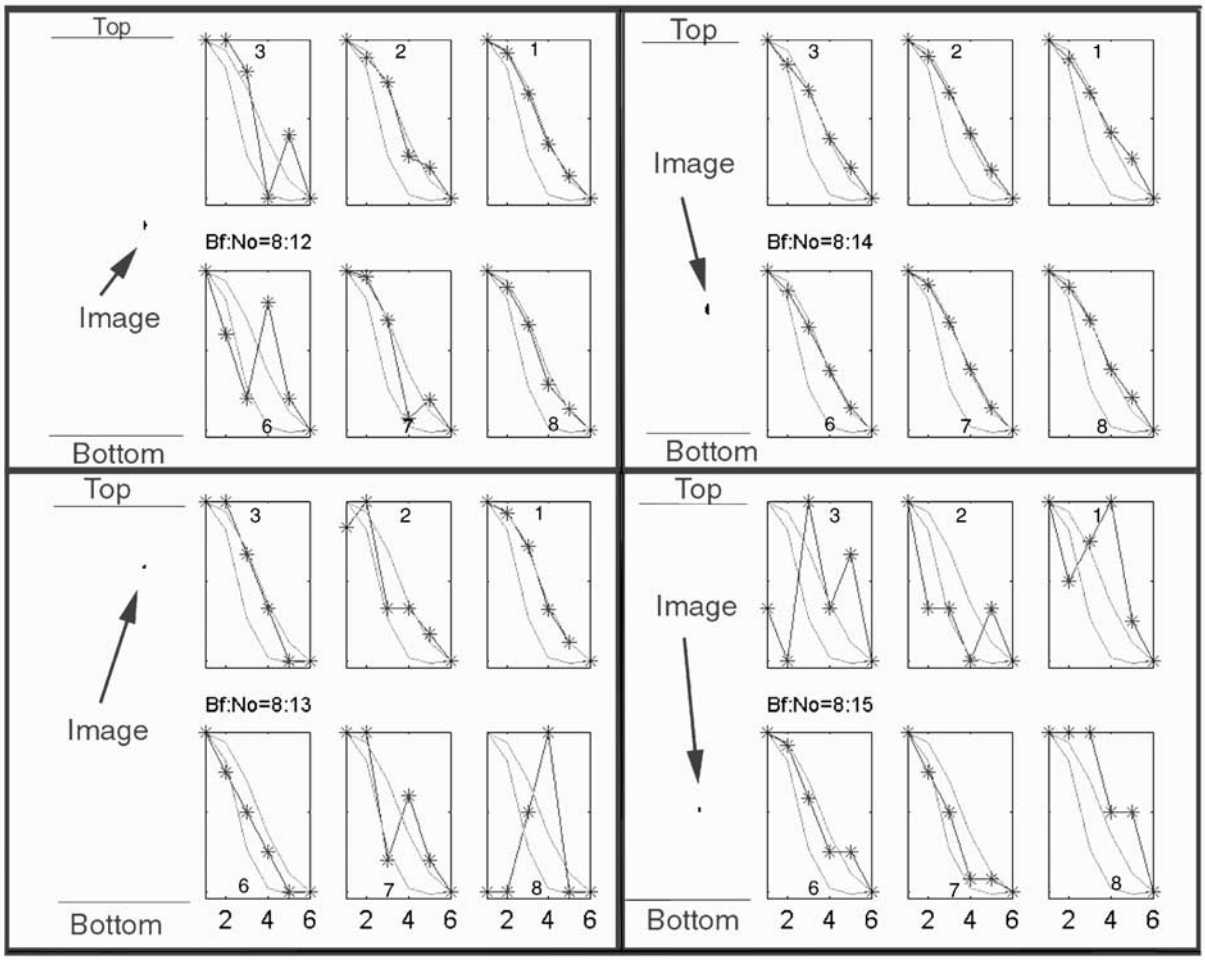

Figure 4. Images of the four particles used in Figure 3 and their normalized, inverted signals along with signals from Figure 2c that form the envelope of curves from the pellet tests. Only the signals from plates 1, 2, 3, 6, 7, and 8 are shown; the other two plates had negligible induced charges because they were far from the particles. The six data points for each electrode are indicated by asterisks. The particle images are positioned to the left of each panel with their vertical positions between panels indicating their approximate positions relative to the top and bottom rows of electrodes.

aft direction, which occurs when the particle is in the laser beam at the time when the particle is first detected and charge sampling is initiated; the ratio was determined empirically using metal pellets whose charge was acquired after leaving the muzzle of a compressed air gun, and then the charge was measured with a special induction ring between the muzzle and the instrument on the airplane.

[24] Figure 2b shows the signals (proportional to induced charge) from all eight electrodes obtained in a laboratory calibration test using metal pellets with a charge of 15 pC. Since the left-right (port-starboard) location of the pellet was between electrode number 3 in the upper row and electrode number 6 in the lower row, the induced charges on these two electrodes were greater than on the other electrodes. The least charges were induced on electrodes 1 and 8, which were farthest from the particle. The induced charges declined after the first of the six samples as the particle moved away from the central fore-aft position in the laser beam.

[25] Figure 2c (left) shows results from 11 pellet tests. The signal from the electrode with the maximum induced charge (closest to the pellet) is shown for each test. The pellets went through the instrument with a variety of different horizontal and vertical locations relative to the electrodes; the location of each pellet was recorded on a paper target behind the electrode array. In Figure 2c (right) all the data points in a single curve (for example, the curve with the dots at the sample times) are multiplied by a constant that makes the value of the signal equal to 1 for the first data point. When this is done for all the curves, the curves look more similar, and are called normalized curves. If a normalized curve during flight in a cloud falls outside the envelope of normalized pellet curves in Figure 2c, then the curve from inside the cloud is rejected as being spurious.

[26] Figure 3 shows the induced charge on all eight electrodes for four different particles. For example, in the top right plot the particle passed between electrodes 2 and 7 and somewhat closer to electrode 7. The induced charges at

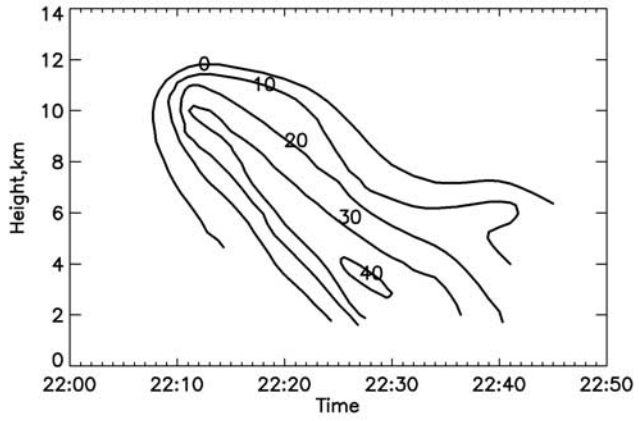

Figure 5. Radar echo time-height diagram showing history of flanking cell. Height is in kilometers above mean sea level (MSL), with the radar itself at 1.43 km. Time is UT. Echo developed first in the 8 to 10 km MSL height range and intensified and descended with time. The aircraft was climbing toward 4 km just after 2235 UT when it encountered the precipitation shaft.

the six sample times at electrodes 2 and 7 have a pattern similar to those of the pellet shown in Figure 2b except that the particle and pellet have charges of opposite sign. The electrodes 1, 3, 6, and 8, which surround electrodes 2 and 7, show a weaker induced charge. Electrodes 4 and 5, which were the most distant from particle, show very little induced charge and very little noise.

[27] In the bottom right plot of Figure 3, the particle passed near the boundary between electrodes 6 and 7, inducing nearly equal charges on both electrodes; the particle was quite close to electrodes 6 and 7 because there is no discernable charge on electrodes 2 and 3. The noise level appears to be greater in the bottom right plot than that in the top right plot because the charge scales on the ordinates have been expanded.

[28] Figure 4 shows normalized curves for the same four particles shown in Figure 3. For comparison, normalized curves have been inverted and plotted together with the curves forming the envelope of the pellet tests. Since large numbers are required to normalize the signal from electrodes with little induced charge, the noise is greatly exaggerated. The electrodes with the most charge have curves similar to those from the pellet tests, except in the bottom right plot, where noise is evident on all the electrodes.

[29] Figure 4 also shows images for the particles and their vertical positions relative to the electrodes. All four particles went through the instrument one after the other with less than 0.05 s between them. For each of the first three particles, the electrode closest to the particle has a signal trace that matches a pellet test signal trace. The signal of the fourth particle matches poorly because the signal is not much larger than the noise.

[30] We used several criteria to discern whether or not a particle carries a calculable charge. In some cases, the signals from several plates are noisy, possibly because of passage of multiple charged particles nearly simultaneously, when the charge on the particle cannot be found and calculation is not possible. In other cases an electrode may acquire a large charge by collision with a particle, such that the electrode's charge was decaying during the passage of one or more subsequent charged particles. In this case, the induced charge cannot be separated from the total charge signal and charge calculation is not possible.

[31] In principle, data analysis and charge calculation can be automated, although the algorithm can get complex as routines are added to deal with all of the factors influencing the observed plate charges. In this study, because the time of passage through the precipitation shaft is short and the total number of particles detected was less than 1000, the computer automatic criteria check algorithm was combined with visual examination of the waveforms from each particle. If the charge data and image data for a particle passed the criteria, the charge was calculated by manually selecting a number of signals. For example, in Figure 3, the charge of particle 12 (top left plot) is calculated as 8 pC, and that of particle 13 (bottom left plot) is 1 pC.

3. Data

[32] On 29 June 2000, a tornadic storm developed in the border region of Kansas, Colorado, and Nebraska. The detailed evolution of the storm from its very beginnings was monitored by the CSU-CHILL and Spol multiparameter radars, the National Weather Service WSR-88D meteorological Doppler radar at Goodland, Kansas, and the NMIMT LMA. *Wiens et al.* [2006] and *Tessendorf et al.* [2005] describe the evolution of this severe storm. The T-28 was launched as this storm became mature. On its way to make its first penetration into the main storm, the T-28 flew under a relatively isolated and collapsing convective cloud, which flanked the tornadic storm. The data presented here are from the passage under this isolated cloud. These data were chosen for detailed study because conditions in the precipitation shaft falling from this cloud were such that charge signals were particularly clean, the cloud history was relatively simple, and the observations show that this region was part of a lower positive charge center, a phenomena of some interest in cloud electrification. In this case, evaluation of the charge measurements and their interpretation in terms of cloud processes can be performed with a higher degree of certainty than data obtained in more chaotic and complex cloud environments encountered later on this flight and on other STEPS flights.

[33] Radar surveillance from the three project radars indicates that a flanking cell developed southwest from the main storm after 2207 UT. The radar-observed cell was isolated from the main storm during all of its evolution. An echo time-height diagram in Figure 5 summarizes the evolution of this cell over about 30 min. The echo first developed between 8 and 10 km and intensified as it fell. The peak reflectivity of 40 dBZ was reached below the melting level after 20 min. By 2230 UT as the main storm strengthened, this region was becoming unfavorable for convective development and the cell was collapsing. A plan view history composed of PPI scans at 7 minute intervals is available as auxiliary material.[1]

[1] Auxiliary materials are available in the HTML. doi:10.1029/2006JD007809.

Figure 6. View from underwing video camera of the cloud producing the precipitation shaft analyzed in this work. The aircraft was climbing toward the northwest toward this cloud and was about 10 km from it at this time.

[34] The T-28 passed under the cell beginning near UT as it climbed northward to line up for a pass through the main storm. Figure 6 shows a video capture from the T-28 of a view of the cloud as the aircraft climbed toward it. Figure 7 is a sector PPI radar scan of the region at 2241 UT showing the arrangement of the main storm and the flanking cell 4 min later. The precipitation shaft that is the focus of this discussion was falling from the nearly circular echo labeled "flanking cell." The irregular echo to the northwest of this one is a remnant from this same cell that was sheared off its top about 20 min earlier and at 2241 is descending through the aircraft flight level.

[35] Figure 8 shows a view of a segment of the aircraft path and the projection onto a horizontal plane of the electric field (E-field) vectors along its path when the aircraft was climbing and was on its way toward the main storm. The two circles along the flight track delimit the precipitation-containing region. The divergent electric field pattern associated with the precipitation region indicates that the region contained positive charge. Figure 9a shows a side view of the aircraft track. The airplane climbed a few hundred meters during the whole time interval shown. The vectors depict the E-field projected onto a vertical plane through the aircraft fuselage. Before **a**, the electric field

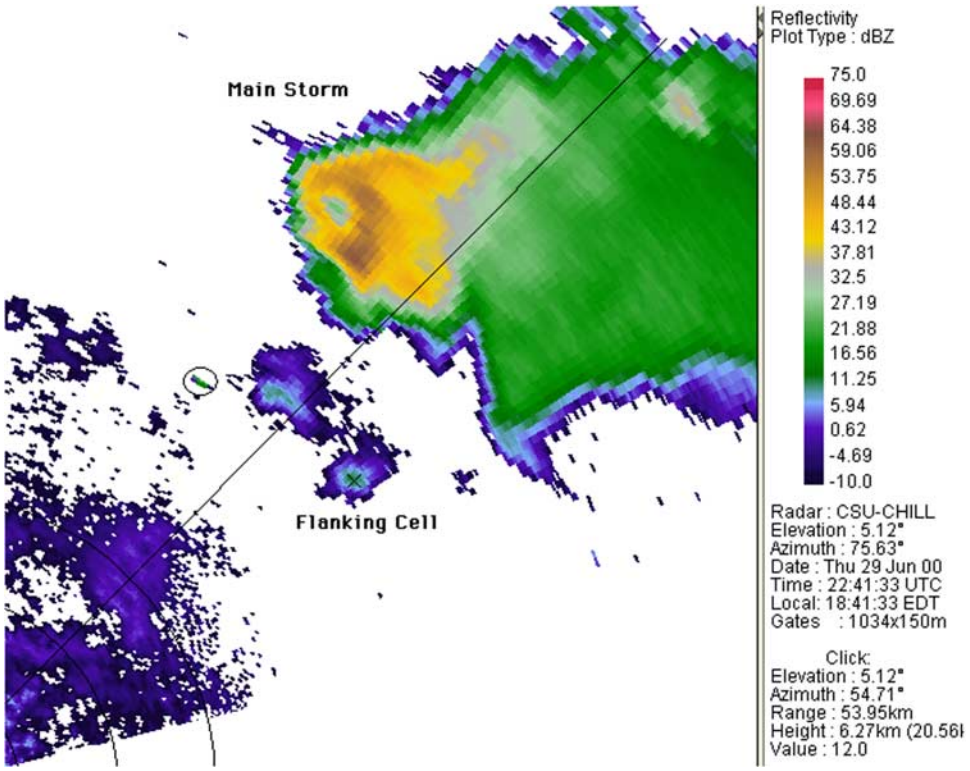

Figure 7. Plan position indicator (PPI) view of radar reflectivity pattern at 2241 UT in the region in which the large storm and flanking cloud developed. The image was obtained 4 min after the T-28 aircraft flew under the feature labeled "flanking cell" near the center of the frame. It climbed under this cell and flew through the echo to the northwest that is a remnant of the top of the flanking cell that separated about 20 min earlier. The echo from the aircraft at this time is circled. Radar reflectivity color scale, time information and view angles are given to the right of the reflectivity image. Range rings with separation 10 km are shown in the lower left corner. In the lower right are given the range, azimuth, altitude (km) and reflectivity value at the location (denoted by a cross) where the radar scanned through the flanking cell near its top.

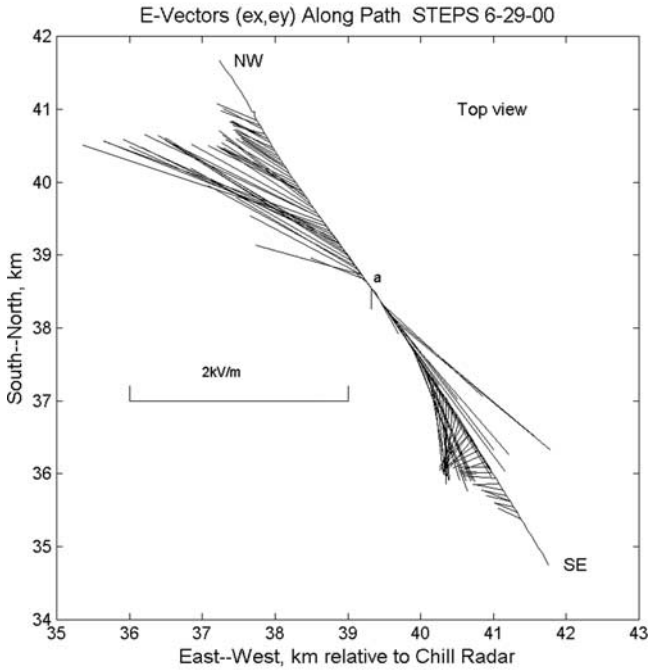

Figure 8. Projections onto a horizontal plane of electric field vectors along the path of the aircraft as it flew through precipitation shaft. Airplane flight direction was from SE to NW. The vector tails are attached to the path of the airplane. The field points from tail to head of each vector. The two circles along the path delimit the boundary of the precipitation region. The electric field reverses direction as aircraft goes through this region, an indication the aircraft has passed a positive charge center.

vectors point downward and are divergent from **a**, suggesting a positive charge center at **a**. As the aircraft climbed higher and passed **a**, the E-field vectors pointed upward and diverged away from **a**; thus both the top view and side view confirm the existence of a region of positive charge surrounding **a**.

[36] Figure 9b shows the magnitudes of the E_x (along track) and E_z (vertical) electric field components along the same segment of track depicted in Figure 9a. In order to make a simple estimate of charge density, we treat the electric field as due to a uniform-density, spherically distributed charge centered on **a.** The peak E_x component of 2.0 kV m^{-1} can be taken to be produced by the sphere charge at its boundary. Assuming the 1.5 km distance between the two E_x peak values as the diameter of the sphere, the charge density is estimated to be 0.07 nC m^{-3}. The total charge in the sphere with these assumptions is 0.1 C.

[37] Figure 9c depicts particle charges as a function of time. During the 20 s when the aircraft passed through the precipitation shaft, the HVPS recorded 886 particle images of which 601 had computable charges. Note that the boundaries of the region containing these charged particles coincide with the maxima of the E_z and E_x field components. This indicates that these precipitation particles are carrying the charge responsible for the observed electric field.

[38] A refinement can be made on the assumption of spherical distribution of charge used above in order to more closely interpret the electric field observations in Figure 9b. A computation of electric fields due to passage through the center of a disk of charge with uniform charge density, shown schematically in Figure 10, shows qualitative agreement with the results shown in Figure 9b. Figure 10 shows E_x and E_z vectors along a track climbing through a disk of charge. Because of symmetry, the E_y field component is zero. The E_x and E_z components are symmetric about the center of the disc. Here the homogeneous disc charge density must be assumed to be positive 0.2 nC/m^3 in order to match the observed electric field E_x component. The total charge inside the disk with these assumptions is 0.07 C. The E_x or E_z components on the left side are negative; at center E_x and E_z are zero, and at the right side E_x and E_z are positive, in agreement with the observations, but these results do not agree quantitatively with the measurements (Figure 9b) where E_z has slightly greater magnitude than E_x. However, the sphere and disk comparisons give us a rough idea of the amount of charge involved.

[39] The 886 particles recorded by the HVPS during the passage through the precipitation shaft were within a sample volume (accounting for electronic dead time) of 10.6 m^3. Of the 886 particles, 601 of them carry computable charges in the range of 0.5 pC to 25 pC, with 587 particles having positive charges and 14 particles having negative charges. All of these 601 particles are confined within the boundaries of the E-field maxima shown in Figure 9b. The remaining 285 particles (32% of the total recorded) either carried charge too small to be detected or charge that was not computable for other reasons. Taking the sum of the 601 particles' charges and dividing by the sample volume, the overall estimated average charge density in the volume sampled by the aircraft is 0.32 nC m^{-3}. This is more than three times the upper estimate based on the electric field measurements and the assumption of a spherical charge distribution, and 60% greater than the average density assuming a disc-like distribution. Thus the assumption of uniform charge density in calculations based on the electric field measurements alone is not accurate.

[40] For the 601 charged particles, the distribution of charge magnitude versus size is shown in Figure 11. (The size distributions of the charged and uncharged particles had similar width, but the mode size of the uncharged particles was 0.5 mm while that of the charged particles was 1 mm.) There is a general trend for larger particles to carry larger minimum and maximum charge, but the charge associated with any one size varies greatly. The scatter is much greater than the uncertainty in charge determination. This is a surprising result if charge is acquired by many collisions in which a small charge is transferred per collision. If each collision transfers the laboratory value of 100 fC [*Jayaratne et al.*, 1983], then 210 collisions would be required to build up the 21 pC charge in the 1.6 mm size range of Figure 11. After 210 collisions, it seems unlikely that one particle would have acquired 21 pC while another particle of the same size acquired only 1.0 pC. Such wide variation in the charge attached to similar-sized particles suggests that considerable charge is transferred in only one or a few

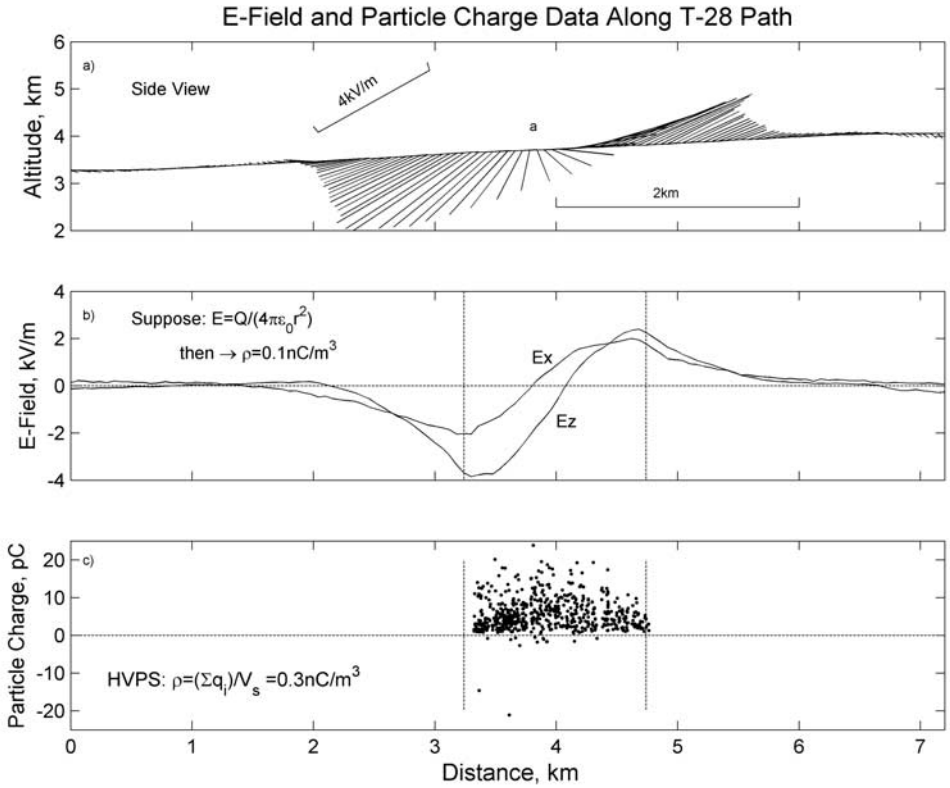

Figure 9. (a) Side view of electric field (E) along the aircraft path. The aircraft flew through the precipitation region under the cloud, centered at *a*, during this portion of its climb. The precipitation region is delineated with vertical dashed lines. The vectors whose tails are attached to the path of the airplane are projections of E onto a vertical plane through the airplane's fuselage. (b) Electric field components along the flight path, E_x, and in the vertical, E_z, during this segment of the flight. (c) Individual precipitation particle charges along the flight path.

collisions, and that charge-transferring collisions are rare. In more recent laboratory experiments [*Jayaratne*, 1999], single collisions between simulated graupel and graupel (rather than graupel and ice crystals) transferred charge approaching 10 pC. This could explain some of the observed variation of charge for a given size.

[41] Another possibility is a melting-charging mechanism. Drake, in 1968, observed melting ice pellets to charge positively in a laboratory experiment. He attributed the net charge to bubbles forming in meltwater, then bursting at the air-liquid surface and ejecting small droplets carrying negative charge. Since the charge separated in the melting process depends strongly on the nature of impurities in the liquid layer, on the thickness of the liquid layer, and on the terminal velocity, perhaps variation of charges on particles with diameters between 1 and 5 mm could be explained by this process. Outside this size range, melting particles would not be expected to separate charge [*Drake*, 1968].

[42] It may be argued that the wide variation of charge with particle size is caused by the fact that the similar-sized particles sampled in proximity to each other came from different parts of the cloud, where charging rates, and even charging directions, were different. As mentioned earlier, it is typically impossible to know the complete history of hydrometeors in a natural cloud, so this possible explanation cannot be conclusively refuted. However, in this case radar observations suggest a simple one-pulse updraft cloud that was collapsing as the aircraft passed beneath it. In such a case, the assumption that the particles sampled along the aircraft trajectory beneath the cloud did have similar cloud-scale growth trajectories may be reasonable. Even given similar trajectories, however, there may have been differences in cloud properties on smaller scales that could have contributed to the broad range of charge magnitudes found on particles with similar sizes.

[43] For particles larger than 1.6 mm, the minimum charge is not zero. There are a few very small particles with charges as large as the largest charges on larger particles. The particle images from the 2D-C and HVPS imaging probes (not shown), and the observed temperature, decreasing from 8°C to 6°C as the aircraft climbed beneath the cloud, lead us to infer that these particles are melting graupel, with the smallest particles probably being completely melted. The HVPS images on this flight have relatively crude resolution, 0.2 mm in the vertical and 0.8 mm in the horizontal. At this resolution, there is no general difference in appearance or size between the many positively charged and few negatively charged particles.

[44] Other aircraft microphysical observations (not shown) are consistent with passage through a weak-intensity precipitation shaft. The heated-coil liquid water

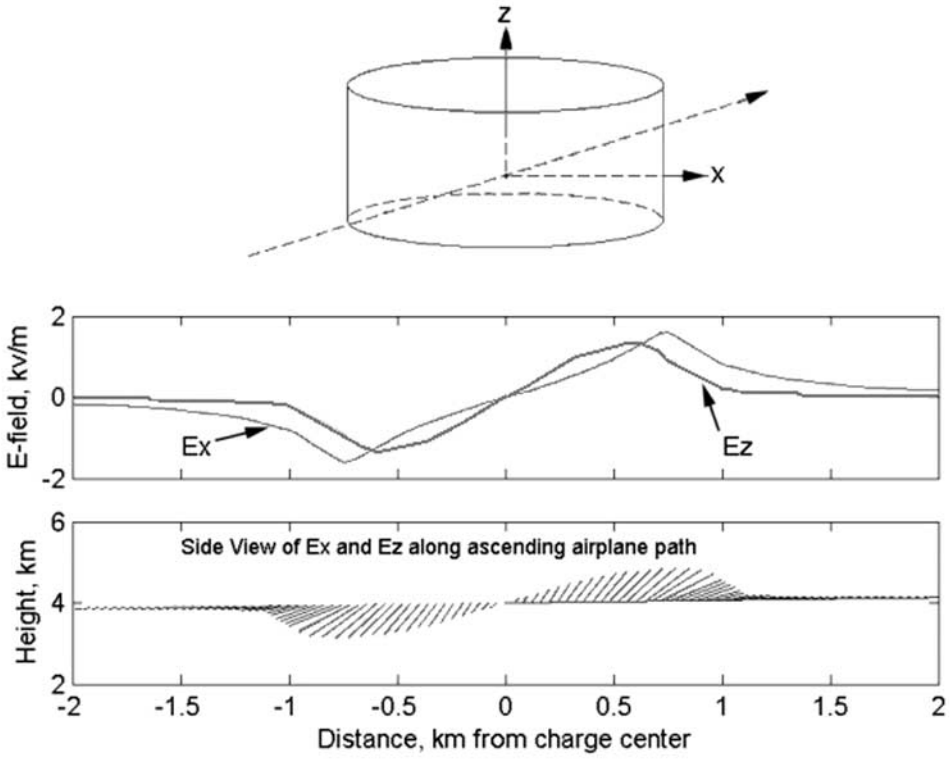

Figure 10. Simulation of E_x and E_z field measured if an airplane is ascending through a charge cylinder. The cylinder (which is 1.5 km in diameter, 210 m in height and is falling at a speed of 3 m/s) has a uniform charge density of 0.2 nC/m^3. At the instant when the airplane distance from the cylinder center is zero, the airplane's path is symmetric about the cylinder. The top sketch shows the relative position of cylinder and airplane path at the instance when the airplane is -0.75 km from the cylinder center. Because of symmetry, E_y is zero. The E_x and E_z components are symmetric about the center. Their values are negative on the left side; at center the values are zero, and at the right side are positive. The E-field pattern shown in Figure 10 (bottom) is similar to the T-28 measurement shown in Figure 7. Of course, the charge region the T-28 went through probably was not as simple as shown in this plot.

instrument response is characterized by a noisy low-magnitude signal due to partial response to precipitation particles in the absence of cloud water. The lack of cloud droplets is confirmed by data from the PMS Forward Scattering Spectrometer Probe (FSSP). The aircraft detected no vertical winds greater than 3 m s^{-1} in magnitude (3 m s^{-1} is the threshold for vertical wind detection using the *Kopp* [1985] technique for calculating vertical winds from aircraft vertical motion). In addition, the LMA and NLDN networks detected no lightning during the entire lifetime of this cloud, consistent with evolution of a cloud that does not develop sufficient vertical depth and convective vigor to separate enough charge to lead to lightning.

4. Discussion

[45] The range of charge density estimates based on the electric field measurements yields a relatively low density of 0.1 to 0.2 nC m^{-3} if the charge is assumed to be distributed in either a spherical or a disc-like volume around the charge center. Charge-density estimates based on these assumptions are the same order of magnitude as the estimate of 0.3 nC m^{-3} based on summing of individual particle charge measurements along the aircraft track. Our result is similar to that of *Marshall and Winn* [1982] and *Bateman et al.* [1999] where they found that in the lower positive charge regions of the storms they observed, the charge was apparently carried entirely by precipitation particles. In our case, we have direct evidence that (1) the only hydrometeors present are precipitation particles and (2) there was no lightning that might have placed charge onto aerosol particles or hydrometeors in the region [see *Mo et al.*, 2002]. In our case, particle charges and volumetric charge densities are lower than those observed by *Marshall and Winn* [1982] and *Bateman et al.* [1999]. Total estimated charge also is lower than in the lower positive charge centers containing $\sim$ 1 C observed by *Winn et al.* [1981] and containing 0.5 to 4 C observed by *Jacobson and Krider* [1976]. It is possible that relatively weaker convection in our case led to reduced particle charging, reduced numbers of charged particles, and subsequently to the lack of sufficient charge separation to trigger lightning.

[46] Because the aircraft is climbing as it passes through the precipitation shaft, the vertical thickness of the charge

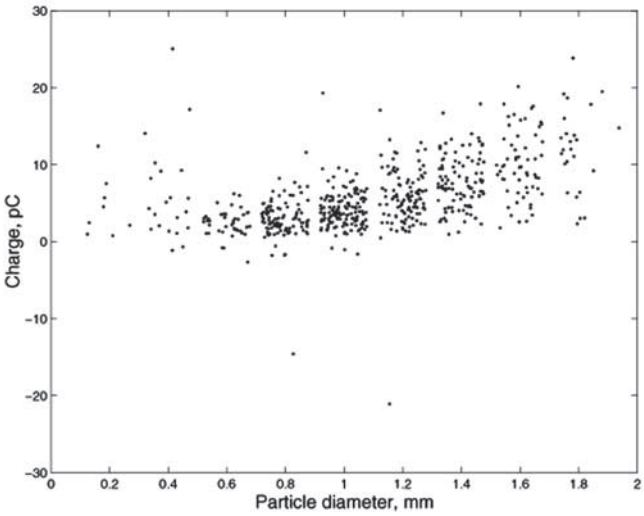

Figure 11. Particle charge versus diameter for 601 charged particles sampled during the 20-s penetration of the small positive charge center. Particle diameter is taken to be the maximum number of shadowed pixels in the vertical direction times 0.2 mm. The particle diameters are digitized in increments of 0.2 mm, but here a random number between −0.08 mm and +0.08 mm has been added to each particle diameter to avoid excessive superposition of dots.

region is shown to be at least 150 m, while it extends horizontally along the aircraft track almost 2 km. The vertical extent, of course, could be much larger than this. Because the vertical extent of the charge region is unknown, there is significant uncertainty in estimating the charge density from the electric field observations in the present case. Because of the uncertain geometry, and the finite region containing charged particles, the simple one-dimensional Gaussian approach to estimating charge density used by *Bateman et al.* [1999], *Stolzenburg and Marshall* [1998], *Marshall and Stolzenburg* [1998], and others, cannot be used here. The precipitation particles carrying charge vary in size from 0.2 to 2.0 mm, with 90% of them between 0.6 to 1.6 mm, consistent with a collection of particles that have undergone similar microphysical histories in a relatively small cloud. Perhaps this similar history leads to the similar charge polarity on the majority of particles.

[47] Radar and visual observations show that this cloud was isolated from the main storm. Although it produced charged particles, the NLDN and LMA detected no lightning discharges within this cloud or from cloud-to-ground. In this case, then, the lower positive charge region found beneath cloud base must have been the result of microphysical interactions within the isolated cloud, and did not result from charge deposited by lightning. The updraft had collapsed and there was no distinct cloud base at the time of the aircraft pass. The temperature at the level of observation was between 8°C and 6°C which is similar to that in the observations by *MacCready and Proudfit* [1965]. The observation of positively charged melting graupel falling below the melting level is similar to that of *MacCready and Proudfit* [1965], suggesting that the observation of positively charged melting graupel falling from marginally electrified clouds may be common. Note, however, that *Latham and Stow* [1969] reported small monopolar regions of both signs, sometimes neighboring oppositely signed monopolar regions beneath the same cloud, while studying a cloud population qualitatively similar to that studied by *MacCready and Proudfit* [1965] and to the cloud described here. See also *Mo et al.* [1998] Figure 9 for a look at charge complexity near cloud base of another cloud in some ways similar to the one observed here. The observation of a uniform region of positive charge on melting graupel below cloud base from weakly electrified clouds is thus certainly not universal.

[48] The instrumentation developed for imaging and simultaneously determining the charge on hydrometeors functioned well in this situation where the mean particle concentration was $\sim$100 m^{-3}. In other more complex environments encountered during the STEPS project, with higher concentrations of a wider range of types and sizes of particles, data interpretation is much more difficult. In these situations it appears that multiple charged particles were present during one particle sampling cycle much of the time. Also, particles may have frequently struck the plates and imparted very large charges that decayed slowly during the passage of several subsequent particles, rendering the computation of particle charge difficult if not impossible. Interpretation of data from these more complex situations is the subject of continued study.

5. Summary

[49] Observations of charged precipitation particles were obtained from an instrumented aircraft that passed through a tenuous precipitation shaft under a small, collapsing, and weakly electrified cloud using a newly developed probe that both images particles and responds to particle electrical charge. This probe is capable of imaging and responding to charge on particles larger than 0.2 mm with charge greater than 0.5 pC. A calibration procedure and algorithm for calculating particle charge is developed and tested. Charge on individual particles with charge greater than a few pC can be determined with an uncertainty of $\sim$13% in optimum conditions, and $\sim$24% in less optimum situations. The range of charge density estimates in the shaft based on the measured E-field along the airplane path agrees to within a factor of 3 with the charge density deduced from the sum of particle charges sampled by the probe along the aircraft path when this sum is divided by the volume sampled by the probe along that path. Peak particle concentrations were $\sim$ 80 m^{-3}. It was found that 68% of the detected precipitation particles carried charge greater than 0.5 pC, the maximum charge was 25 pC, and 98% of the charged particles were charged positively. Particles having the same size carried a range of magnitudes of charge, but minimum, maximum, and mean charge magnitude generally increased with particle size. No distinct difference was found in appearance or size between positively and negatively charged particles. The lack of lightning throughout the cloud life cycle implies that microphysical processes and not lightning deposition are responsible for this observed lower positive charge center.

[50] This work demonstrates the successful operation of a new instrument capable of imaging particles while simultaneously collecting information on particle charge. Further

refinements in data interpretation techniques are needed to better understand observations obtained during passage through mixed phase regions in STEPS thunderstorm interiors with much higher particle and charge concentrations than those encountered here.

[51] **Acknowledgments.** This work was supported by grants ATM 9981175 and ATM 0099344 from the National Science Foundation to the South Dakota School of Mines and Technology and grants ATM 9318887 and ATM 0070934 to the New Mexico Institute of Mining and Technology. Additional support came from the State of South Dakota. Thanks to Connie Crandall for editing and manuscript preparation; to SPEC, Inc., for working with us on modifications to their HVPS probe; and to Donna Kliche and Rand Feind for software development.

References

Bateman, M. G., W. D. Rust, and T. C. Marshall (1994), A balloon-borne instrument for measuring charge and size of precipitation particles inside thunderstorms, *J. Atmos. Oceanic Technol.*, *11*, 161–169.

Bateman, M. G., W. D. Rust, B. F. Smull, and T. C. Marshall (1995), Precipitation charge and size measurements in the stratiform region of two mesoscale convective systems, *J. Geophys. Res.*, *100*, 16,341–16,356.

Bateman, M. G., T. C. Marshall, M. Stolzenburg, and W. D. Rust (1999), Precipitation charge and size measurements inside a New Mexico mountain thunderstorm, *J. Geophys. Res.*, *104*, 9643–9653.

Bringi, V. N., K. Knupp, A. Detwiler, L. Liu, I. J. Caylor, and R. A. Black (1997), Evolution of a Florida thunderstorm during the convection and precipitation/electrification experiment: The case of 9 August 1991, *Mon. Weather Rev.*, *125*, 2131–2160.

Brooks, I. M. (1993), Laboratory studies of thunderstorm charging processes, Ph.D. Dissertation, 164 pp., Phys. Dep., Univ. of Manchester, Manchester, U. K.

Brunkow, D., V. N. Bringi, P. C. Kennedy, S. A. Rutledge, V. Chandrasekar, E. A. Mueller, and R. K. Bowie (2000), A description of the CSU-CHILL national radar facility, *J. Atmos. Oceanic Technol.*, *17*, 1596–1608.

Christian, H., C. R. Holmes, J. W. Bullock, W. Gaskell, A. J. Illingworth, and J. Latham (1980), Airborne and ground-based studies of thunderstorms in the vicinity of Langmuir Laboratory, *Q. J. R. Meteorol. Soc.*, *106*, 159–174.

Cupal, J. J., N. R. Kale, P. J. Wechsler, and G. Vali (1989), An instrument for the simultaneous measurement of the image and electric charge of hydrometeors, *J. Atmos. Oceanic Technol.*, *6*, 697–705.

Drake, J. C. (1968), Electrification accompanying the melting of ice particles, *Q. J. R. Meteorol. Soc.*, *94*, 176–191.

Dye, J. E., J. J. Jones, W. P. Winn, T. A. Cerni, B. Gardiner, D. Lamb, R. L. Pitter, J. Hallett, and C. P. R. Saunders (1986), Early electrification and precipitation development in a small, isolated Montana cumulonimbus, *J. Geophys. Res.*, *91*, 1231–1247.

Fong, C. Y., and C. Kittel (1967), Induced charge on capacitor plates, *Am. J. Phys.*, *35*, 1091–1097.

Gardiner, B., D. Lamb, R. L. Pitter, and J. Hallett (1985), Measurements of initial potential gradient and particle charges in a Montana thunderstorm, *J. Geophys. Res.*, *90*, 6079–6086.

Gaskell, W., A. J. Illingworth, J. Latham, and C. B. Moore (1977), Airborne studies of thunderstorm electrification, *Nature*, *268*, 124–125.

Gaskell, W. A., A. J. Illingworth, J. Latham, and C. B. Moore (1978), Airborne studies of electric fields and the charge and size of precipitation elements in thunderstorms, *Q. J. R. Meteorol. Soc.*, *104*, 447–460.

Gunn, R. (1947), The electrical charge on precipitation at various altitudes and its relation to thunderstorms, *Phys. Rev.*, *71*(3), 181–186.

Jacobson, E. A., and E. P. Krider (1976), Electrostatic field changes produced by Florida lightning, *J. Atmos. Sci.*, *33*, 103–117.

Jayaratne, E. R. (1999), Separation of charge during rebounding collisions between graupel as a possible mechanism of thunderstorm electrification, in *Proceedings of the 11th International Conference on Atmospheric Electricity, Guntersville, Alabama*, *NASA Rep. NASA/CP-1999-209261*, 308–311.

Jayaratne, E. R., C. P. R. Saunders, and J. Hallett (1983), Laboratory studies of the charging of soft hail during ice crystal interactions, *Q. J. R. Meteorol. Soc.*, *109*, 609–630.

Johnson, G. N., and P. L. Smith Jr. (1980), Meteorological instrumentation system on the T-28 thunderstorm research aircraft, *Bull. Am. Meteorol. Soc.*, *61*, 972–979.

Kopp, F. J. (1985), Deduction of vertical motion in the atmosphere from aircraft measurements, *J. Atmos. Oceanic Technol.*, *2*, 684–688.

Krehbiel, P. R. (1986), The electrical structure of thunderstorms, in *The Earth's Electrical Environment*, pp. 90–113, Natl. Acad. Press, Washington, D. C.

Latham, J., and C. D. Stow (1969), Airborne studies of the electrical properties of large convective clouds, *Q. J. R. Meteorol. Soc.*, *95*, 486–500.

MacCready, P. B., and A. Proudfit (1965), Observations of hydrometeor charge evolution in thunderstorms, *Q. J. R. Meteorol. Soc.*, *91*, 44–53.

MacGorman, D. R., and W. D. Rust (1998), *The Electrical Nature of Storms*, pp. 118–162, Oxford Univ. Press, New York.

Marshall, T. C., and W. P. Winn (1982), Measurements of charged precipitation in a New Mexico thunderstorm: Lower positive charge centers, *J. Geophys. Res.*, *87*, 7141–7157.

Marshall, T. C., and M. Stolzenburg (1998), Estimates of cloud charge densities in thunderstorms, *J. Geophys. Res.*, *103*, 19,769–19,775.

Mo, Q., A. Ebneter, P. Fleishhacker, and W. P. Winn (1998), Electric field measurement with an airplane: A solution to problems caused by emitted charge, *J. Geophys. Res.*, *103*, 17,163–17,173.

Mo, Q., R. E. Feind, F. J. Kopp, and A. G. Detwiler (1999), Improved electric field measurements with the T-28 armored research airplane, *J. Geophys. Res.*, *104*, 24,485–24,497.

Mo, Q., J. H. Helsdon Jr., and W. P. Winn (2002), Aircraft observations of the creation of lower positive charges in thunderstorms, *J. Geophys. Res.*, *107*(D22), 4616, doi:10.1029/2002JD002099.

Reynolds, S. E., M. Brook, and M. F. Gourley (1957), Thunderstorm charge separation, *J. Meteorol.*, *14*, 426–436.

Rison, W., R. J. Thomas, P. R. Krehbiel, T. Hamlin, and J. Harlin (1999), A GPS-based three-dimensional lightning mapping system: Initial observations in central New Mexico, *Geophys. Res. Lett.*, *26*, 3573–3576.

Saunders, C. P. R., W. D. Keith, and R. P. Mitzeva (1991), The effect of liquid water on thunderstorm charging, *J. Geophys. Res.*, *96*, 11,007–11,017.

Stolzenburg, M., and T. C. Marshall (1998), Charged precipitation and electric field in two thunderstorms, *J. Geophys. Res.*, *103*, 19,777–19,789.

Stolzenburg, M., W. D. Rust, and T. C. Marshall (1998), Electrical structure in thunderstorm convective regions: 2. Isolated storms, *J. Geophys. Res.*, *103*, 14,079–14,096.

Takahashi, T. (1978), Riming electrification as a charge generating mechanism in thunderstorms, *J. Atmos. Sci.*, *35*, 1536–1548.

Tessendorf, S. A., L. J. Miller, K. C. Wiens, and S. A. Rutledge (2005), The 29 June 2000 supercell observed during STEPS. Part I: Kinematics and microphysics, *J. Atmos. Sci.*, *62*, 4127–4150.

Vali, G., J. Cupal, C. P. R. Saunders, and W. P. Winn (1984), Airborne measurements of the electrical charge of hydrometeors, paper presented at Ninth International Cloud Physics Conference, Int. Assoc. of Meteorol. and Atmos. Phys., Tallinn, Estonia.

Weinheimer, A. J., J. E. Dye, D. W. Breed, M. P. Spowart, J. L. Parrish, and T. L. Hoglin (1991), Simultaneous measurements of the charge, size, and shape of hydrometeors in an electrified cloud, *J. Geophys. Res.*, *96*, 20,809–20,829.

Wiens, K. C., S. A. Tessendorf, and S. A. Rutledge (2006), The 29 June 2000 supercell observed during STEPS. Part II: Lightning and charge structure, *J. Atmos. Sci.*, *62*, 4151–4177.

Williams, E. R. (1989), The tripole structure of thunderstorms, *J. Geophys. Res.*, *94*, 13,151–13,167.

Winn, W. P., C. B. Moore, and C. R. Holmes (1981), Electric field structure in an active part of a small, isolated thundercloud, *J. Geophys. Res.*, *86*, 1187–1193.

G. Aulich, Langmuir Laboratory, New Mexico Institute of Mining and Technology, Langmuir Laboratory, 801 Leroy Place, Socorro, NM 87801-4796, USA.

A. G. Detwiler and J. Helsdon, Institute of Atmospheric Sciences, South Dakota School of Mines and Technology, 501 East St. Joseph Street; Rapid City, SD 57701, USA. (andrew.detwiler@sdsmt.edu)

Q. Mo, SPEC, Inc., 3022 Sterling Circle, Suite 200, Boulder, CO 80301, USA.

W. C. Murray, Department of Mathematics and Statistics, University of New Mexico, Valencia Campus, Los Lunas, NM 87031, USA.

W. P. Winn, Department of Physics, New Mexico Institute of Mining and Technology, Langmuir Laboratory, 801 Leroy Place, Socorro, NM 87801-4796, USA.